Journal of Biomedical Optics 7(3), 457–463 (July 2002)

In vivo human retinal imaging by Fourier domain optical coherence tomography

Maciej Wojtkowski
Nicholas Copernicus University
Institute of Physics
ul. Grudziadzka 5/7
Pl-87-100 Torun, Poland

Rainer Leitgeb
University of Vienna
Institute of Medical Physics
Waehringer Strasse 13
A-1090 Wien, Austria

Andrzej Kowalczyk
Tomasz Bajraszewski
Nicholas Copernicus University
Institute of Physics
ul. Grudziadzka 5/7
Pl-87-100 Torun, Poland

Adolf F. Fercher
University of Vienna
Institute of Medical Physics
Waehringer Strasse 13
A-1090 Wien, Austria

Abstract. We present what is to our knowledge the first *in vivo* tomograms of human retina obtained by Fourier domain optical coherence tomography. We would like to show that this technique might be as powerful as other optical coherence tomography techniques in the ophthalmologic imaging field. The method, experimental setup, data processing, and images are discussed. © *2002 Society of Photo-Optical Instrumentation Engineers.* [DOI: 10.1117/1.1482379]

Keywords: OCT; Fourier domain OCT; ophthalmic instruments.

Paper JBO-01066 received Oct. 2, 2001; revised manuscript received Jan. 9, 2002; accepted for publication Jan. 14, 2002.

1 Introduction

Tomographic retinal imaging *in vivo* as well as the measurement of the thickness of retinal layers plays an important role in contemporary ophthalmic diagnosis. Instruments and techniques like scanning laser ophthalmoscopy,[1] ultrasonography,[2] or partial coherence interferometry[3] (PCI) are successfully used in ophthalmic clinics. Competitive optical coherence tomography (OCT) joined the earlier-mentioned methods in the past 12 years.[4] The micron longitudinal resolution, high sensitivity, precision, and noncontact operations are responsible for the success of this technique in retinal imaging.

Huang et al. reported the first tomogram of the human retina *in vitro* in 1991.[5] The first OCT tomogram of the human optic disk *in vivo* was presented in 1993 by Fercher et al.[6] The first macular imaging *in vivo* done by Swanson et al.[7] in 1993 and pathological retinal tomograms *in vivo* were performed shortly afterwards.[8] Since then OCT has advanced as a powerful imaging modality for clinical applications demonstrating the detection and monitoring of macular diseases[9–11] as well as early glaucoma diagnosis[12] capabilities. The visualization of morphologic features of human retina structures (macula, optic disk) as well as the precise quantification of the retinal nerve fiber layer thickness are the most desirable parameters in ophthalmic early diagnosis.

The next step in the ophthalmic application of OCT is the development of functional OCT, which allows for the measurement of spatially resolved blood oxygenation. It can be realized by spectroscopically sensitive techniques. The first, preliminary, results of spectroscopically sensitive OCT based on a time domain OCT setup were reported by Drexler et al.[13] in 2000. In the same year Leitgeb et al.[14] published preliminary results with a method based on Fourier domain OCT technique. This OCT modality inherently provides direct access to spectral information and is thus a promising candidate for the assessment of functional parameters. The earlier-mentioned method is called Fourier domain optical coherence tomography (FDOCT). The idea and first Fourier domain optical A scans (PCI) *in vivo* were presented in 1995 by Fercher et al.,[15] but retinal images have not been obtained with FDOCT up to date. An advantage of FDOCT in comparison to time domain OCT is the elimination of a moving reference, which gives the potential of high speed imaging.[16] The principles of FDOCT were previously used in other axial scan free techniques like spectral radar,[17,18] wavelength tuning interferometry,[19] chirp OCT,[20] and grating generated scanning coherence microscopy.[21] However, to our knowledge nobody has used them in retinal imaging yet.

In this paper we describe a modified version of the FDOCT method. With this method it is possible to avoid parasitic terms resulting from mutual interferences of waves reflected at different object depths. We present its potential to image the morphology of the human retina as well as to provide quantitative information about retinal layer thicknesses.

2 Experimental Setup

The FDOCT instrument is able to access the depth information (optical A scan) of an object without any mechanical scanning parts. The interference pattern after the grating as recorded by the charge coupled device (CCD) camera carries the information about the distribution of reflecting layers in

Address all correspondence to Maciej Wojtkowski. Tel.: ++48-56-611-33-15; Fax: ++48-56-622-53-97; E-mail: max@phys.uni.torun.pl

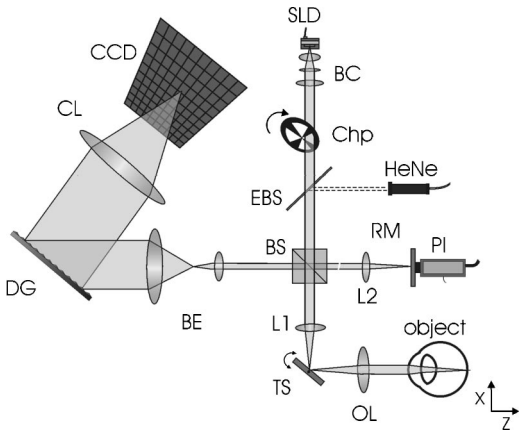

Fig. 1 Optical scheme of the Fourier domain spectral OCT device: SLD superluminescent diode, BC collimator, EBS edge beam splitter, Chp optical chopper, HeNe helium-neon laser, RM reference mirror, PI piezotranslator, BS beam splitter, OL objective lens, L_1, L_2 lenses, TS transversal scanner, BE beam expander, DG diffraction grating, CL camera objective, CCD camera.

the object along the illuminating beam. The acquired data have to be Fourier transformed, in order to create an optical A scan. A two-dimensional reconstruction of a tissue volume is possible by additional transverse scanning of the illuminating beam.

An interferometer, the main part of the FDOCT instrument, is based on an open air Michelson interferometer setup (Figure 1) with a 50/50 cube beam-splitter (Linos). A superluminescent diode (Superlum) acts as a temporally low and spatially high coherent light source emitting at 810 nm with a 20 nm full width at half maximum (FWHM) and a maximal output power of 2 mW. The detection unit consists of a diffraction grating (1800 grooves/mm Spectrogon) and a 18-bit cooled CCD camera (Andor Technologies, 64 kHz sampling rate of frame grabber, 16 bit analog to digital conversion, 1024×128 pixels, 27×27 μm pixel size, full vertical binning). In order to introduce a phase shift into the reference beam, which is needed for the differential FDOCT, the reference mirror is mounted on a piezotranslator (Physik Instrumente). A helium–neon laser serves for beam adjustment and aiming. The losses at the spectrometer are approximately equal to 20%.

Lenses OL, $f=12$ mm and L1 with the focal length $f=80$ mm create an inverted beam expander system. Such a configuration ensures that a parallel beam, which illuminates the cornea, is eventually focused by the eye onto the retina. The fixing light is situated more than 1 m from the subject. The pivot of the transverse scanner (Cambridge Technology) is imaged in the plane of the patient's pupil by the lens OL. Such arrangement provides maximal scanning range for a given OL aperture. The OL lens serves as the objective with the numerical aperture$=0.42$.

The transversal point-spread function is approximately $\Delta x=30$ μm. The focal depth theoretically estimated for an optical system of the eye is $\Delta z>1$ mm. The optical power of the incident beam at the cornea is $P=130$ μW, this value is consistent with the ANSI recommended exposure limit for continuous direct beam viewing.[22] The transfer time (19 ms) between CCD and personal computer is much longer than the time required to collect the spectrum (1 ms). The transfer time increases the total measurement time causing several problems connected with eye movements. The model of CCD employed in our FDOCT instrument is not equipped with a shutter, therefore any eye movement during the transfer time causes the spectral fringes to be blurred, of deteriorated visibility. As an effective countermeasure the sector rotating at 50 Hz was introduced to block the light for the image transfer time. After the transfer of the acquired spectra to a personal computer, data are processed and visualized by software written in LabView.

3 Basic Principles

The technique of Fourier domain OCT is based on spectral interferometry, i.e., interference of broadband light waves registered by a spectrometer. A beam originating from a light source is split into two partially coherent beams. One beam penetrates the object along the z axis, and is reflected back from the nth scattering center with the real-valued backscattering coefficient $\alpha_n(\nu)$:

$$u_n=u(t+2\tau_n)=\int_{-\infty}^{+\infty}S_0(\nu)\sqrt{\alpha_n(\nu)}\exp[-2\pi i\nu(t+2\tau_n)]d\nu, \quad (1)$$

where $S_0(\nu)$ is the amplitude spectral distribution of the light source. A second beam is reflected from the reference mirror

$$u_r=u(t+2\tau_r)=\int_{-\infty}^{+\infty}S_0(\nu)\sqrt{\alpha_r(\nu)}\exp[-2\pi i\nu(t+2\tau_r)]d\nu, \quad (2)$$

where $\alpha_r(\nu)$ is the reflection coefficient.

The earlier two beams are delayed by $2\tau_n$ and $2\tau_r$, where delay times $\tau=z/c$ are related to the location of each (nth) scattering center by the initial position of the reference mirror and to the beam splitter position respectively. Resulting interference is recorded as a function of frequency

$$G_{UU}(\nu)=G^{rr}(\nu)+\sum_n G^{nn}(\nu)+2\,\mathrm{Re}\left\{\sum_{n\neq m}G^{nm}(\nu)\exp[-4\pi i\nu(\tau_n-\tau_m)]\right\}+2\,\mathrm{Re}\left\{\sum_n G^{nr}(\nu)\exp[-4\pi i\nu(\tau_n-\tau_r)]\right\}, \quad (3)$$

$$\text{where: } G^{nm}(\nu)\equiv\lim_{T\to\infty}\left[\frac{\overline{U^m(\nu)U^{n*}(\nu)}}{2T}\right] \quad (4)$$

is called spectral density function,[23] and

$$U^m(\nu)=FT[u(t+\tau_m)]=S_0(\nu)\sqrt{\alpha_m(\nu)}\exp(-2\pi i\nu\tau_m) \quad (5)$$

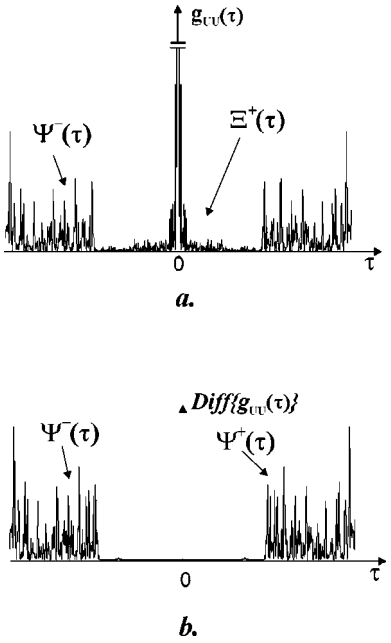

Fig. 2 Optical A scans of the same sample obtained by: (a) FDOCT technique and (b) differential technique.

is the amplitude spectral distribution. The module of each spectral density function will be equal to the intensity spectral distribution of the light source modified by and/or, reflection, or scattering coefficients

$$|G^{mn}(\nu)| = S_0(\nu)S_0^*(\nu)\sqrt{\alpha_n(\nu)\alpha_m(\nu)} = I(\nu)\sqrt{\alpha_n(\nu)\alpha_m(\nu)}. \quad (6)$$

Fourier transformation of the spectral density function $G_{UU}(\nu)$ yields

$$FT^{-1}[G_{UU}(\nu)] = FT^{-1}[G^{rr}(\nu)] + \sum_n FT^{-1}[G^{nn}(\nu)] + 2\sum_{n\neq m} FT^{-1}\{|G^{nm}(\nu)| \times \cos[4\pi\nu(\tau_n-\tau_m)]\} + 2\sum_n FT^{-1}\{|G^{nr}(\nu)| \times \cos[4\pi\nu(\tau_n-\tau_r)]\}. \quad (7)$$

According to the Wiener–Khinchin theorem, there is a correspondence between the spectral density function and the complex first-order electric field correlation function[24] $\Gamma(\tau_n) \equiv \langle u(t)u^*(t+\tau_n)\rangle$:

$$\Gamma(\tau) = FT^{-1}[G(\nu)]. \quad (8)$$

Applying this theorem to Eq. (7), one obtains

$$g_{UU}(\tau) = FT^{-1}[G_{UU}(\nu)] = \Gamma^{rr}(\tau) + \sum_n \Gamma^{nn}(\tau) + \Xi^+(\tau) + \Xi^-(\tau) + \Psi^+(\tau) + \Psi^-(\tau). \quad (9)$$

The total signal described in Eq. (9) consists of the following terms [Figure 2(a)]: The first two terms correspond to the intensities of the reflected reference beam and of beams reflected from layers distributed within the object. The following two terms are associated with the interference of all elementary waves reflected back from different object interfaces

$$\Xi^{\pm}(\tau) = \sum_{n\neq m} \Gamma[\tau \pm 2(\tau_m - \tau_n)]. \quad (10)$$

Earlier mentioned terms are called by other authors as autocorrelation terms.[25]

The last two terms originate from intereference between reflected object waves and the reflected wave from the reference mirror

$$\Psi^{\pm}(\tau) = \sum_n \Gamma[\tau \pm 2(\tau_r - \tau_n)]. \quad (11)$$

Only the terms included in $\Psi^{\pm}(\tau)$ provide direct information on the positions of reflecting layers with respect to the constant position of the reference mirror. Unfortunately, all six terms mix, what precludes the interpretation of the data. In the simplest way one can separate the terms containing useful information from the parasitic ones by shifting of the reference mirror by a distance larger than the optical thickness of the sample. Unfortunately, such a procedure reduces the working depth range.

The differential Fourier domain method (dFDOCT) employs the fact that terms carrying direct information on the location of reflecting layers depend on the reference mirror position while the remaining parasitic terms do not. In order to completely remove the parasitic terms it is sufficient to measure one additional spectrum $G_{UU}(\nu)$, with a phase shift π introduced into the reference arm.

After subtraction of these two spectra, one yields terms associated exclusively with the object structure

$$\mathrm{Diff}[G_{UU}^{[1]}(\nu)] = G_{UU}^{[1]}[\phi(\nu)] - G_{UU}^{[2]}[\phi(\nu)+\pi] = 4\sum_n |G^{nr}(\nu)|\cos[4\pi\nu(\tau_n-\tau_r)] = 4\sum_n \mathrm{Re}[G^{nr}(\nu)]. \quad (12)$$

Fourier transformation of 4 $\mathrm{Re}[G^{nr}(\nu)]$ results in the expression

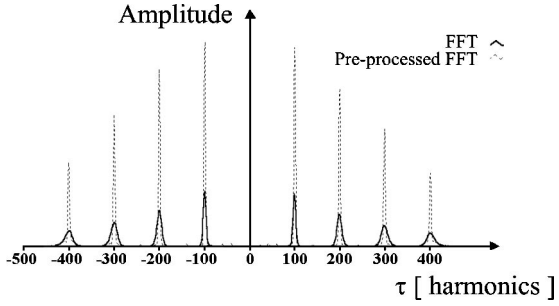

Fig. 3 The set of overlapped optical A scans measured for different optical distances between the reference mirror and an object (mirror). Data were processed by the FFT (line) and by the scaling algorithm followed by FFT (dashed line).

$$\begin{aligned}\mathrm{Diff}[g_{UU}(\tau)] &= FT^{-1}\{4\,\mathrm{Re}[G^{nr}(\nu)]\}\\ &= 2\sum_n \Gamma[\tau + 2(\tau_r - \tau_n)]\\ &\quad + 2\sum_n \Gamma[\tau - 2(\tau_r - \tau_n)] = 2\Psi^{\pm}(\tau),\end{aligned} \tag{13}$$

which is free of the parasitic terms [Figure 2(b)].

4 Measurement Range, Resolution and Dynamic Range

The measurement range of the FDOCT device depends on the spectral resolution of the spectrometer. Practically the useful information about the object structure is deciphered by the numerical Fourier transform (FFT) of the measured signal. The number of sampling points N is given by the number of illuminated CCD pixels. The dependence between the jth harmonic and the optical path difference ℓ_j is the following:

$$\ell_j = \frac{1}{2n}\frac{\lambda_0^2}{\Delta\lambda} j, \quad j = 1,2,\ldots,N/2, \tag{14}$$

where n is the refractive index and $\Delta\lambda$ is the registered width of the spectrum. According to the Nyquist condition the index of the maximum harmonics is equal to $N/2$. Therefore the maximum path difference registered by a FDOCT device is

$$\ell_{\max} = \frac{1}{4n}\frac{\lambda_0^2}{\Delta\lambda} N. \tag{15}$$

In our FDOCT setup $n\ell_{\max}$ amounts to approximately 3.5 mm. The longitudinal resolution in the FDOCT method is dependent on the coherence length of the light source ℓ_c, and is defined as

$$\delta z = \frac{\ell_c}{2} = \frac{2\ln 2}{\pi n}\frac{\lambda_0^2}{\mathrm{FWHM}(\lambda)}. \tag{16}$$

Combination of Eqs. (14) and (16) allows to calculate the FWHM of the axial point spread function (PSF) in terms of harmonic

$$\delta z^{(j)} = \frac{4\ln 2}{\pi}\frac{\Delta\lambda}{\mathrm{FWHM}(\lambda)}. \tag{17}$$

In our case, where $\Delta\lambda > 2\mathrm{FWHM}$ we obtain $\delta z^{(j)} = 2$harmonics. The data collected by the spectrometer are sampled with equal wavelength increments. Fourier transform, however, links z and k spaces (or τ and ω). Because of the nonlinear relation between k and λ the Fourier transform of data acquired directly from the spectrometer is improper. The signal is evenly sampled in λ space but unevenly sampled in k space. This will lead to a broadening of the PSF function with the increase of the optical distance between an object and the reference arm, even for a simple reflecting surface placed in the object arm (Figure 3). In order to compensate this effect preprocessing of the recorded data is needed before taking the numerical FFT. We used first a nonlinear scaling algorithm, which transforms evenly sampled spectrum in λ into an evenly sampled signal in k. The axial resolution as well as the amplitude were improved (Figure 3). The observed decay of the amplitude at variable distance in the Figure 3 is caused by the limited spectral resolution of the spectrometer.[25]

The important features of every OCT system, which characterize the measurement performance, are dynamic range and signal-noise ratio. The dynamic range (DR) and the maximal signal to noise ratio $[(\mathrm{S/N})_{\max}]$ are related by:[26] $\mathrm{DR} = 10\log[(\mathrm{S/N})_{\max}]$, where signal to noise ratio is defined as the ratio of the minimum to the maximum measurable photocurrent power P, which is proportional to I^2:

$$(\mathrm{S/N})_{\max} = \frac{P_{\max}}{P_{\min}}. \tag{18}$$

For shot-noise limited detection the maximal signal to noise ratio of the CCD is proportional to the saturation level of each pixel given by the full well capacity (FWC):[27]

$$(\mathrm{S/N})_{\max} = \mathrm{FWC}. \tag{19}$$

The dynamic range is given by the following formula:[28]

$$\mathrm{DR} = 10\log\left(\frac{[Pt]_{\max}\eta}{2Nh\nu}\right), \tag{20}$$

where P is the optical power from the object, t is the exposure time, $[Pt]_{\max}$ is the saturation energy of N illuminated pixels, η is the quantum efficiency, h is the Planck constant, and ν is the central frequency of the incident light wave. The Fourier transformation of the signal acts as a narrow bandpass filter.[27] As was mentioned earlier the FWHM of the axial point spread function equals 2 harmonics. Hence, the Fourier transformation is ''compressing'' whole useful information into two harmonics since the white noise is distributed after FFT over $N/2$ harmonics, the maximum signal to noise ratio is increased by factor $N/4$:

$$\mathrm{DR}^{\mathrm{FDOCT}} = 10\log\left(\frac{[Pt]_{\max}\eta}{8h\nu}\right) = 10\log\left(\frac{\mathrm{FWC}N}{8}\right). \tag{21}$$

The theoretically estimated value for the DR of Fourier domain OCT amounted to 79 dB.

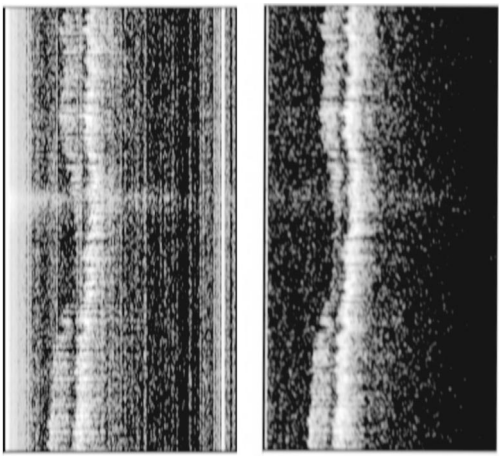

Fig. 4 Two tomograms of human macula region *in vivo* obtained with standard (left panel) and differential (right panel) FDOCT techniques. In both panels the same greyscale is used.

In order to estimate the DR value experimentally we used a mirror in the object arm and gradually attenuated the object beam by a set of neutral density filters, while the reference intensity was left fixed at half of the saturation level. The DR was calculated as the ratio of the optical power corresponding to camera saturation to the optical power, at which interference fringes were still distinguishable from the noise. Thus we obtained $DR_{exp}^{FDOCT} = 67$ dB. Clearly the parasitic autocorrelation terms and flicker noise decrease the dynamic range. In order to improve the dynamic parameters of FDOCT we used a differential technique, which reduces the correlated component of the noise background, which results from the $\Xi^{\pm}(\tau)$ terms in Eq. (9). The dynamic range measured for the differential method is $DR_{exp}^{dFDOCT} = 71$ dB. Therefore, the signal to noise ratio is enhanced due to the differential technique by a factor of ~ 1.6 times.

5 Retinal Measurements

Figure 4 presents a comparison between two tomograms of the human retina *in vivo* obtained with the standard and differential FDOCT techniques. The autocorrelation (parasitic) terms are strongest for small fringes frequencies, i.e., close to the zero path difference, (left panel in Figure 4). However, for longer optical distances one can still observe some autocorrelation terms (regular vertical stripes) originating from the interference between the rays reflected back from different optical components in the instrument. The differential technique efficiently reduces all these artifacts and uncovers the morphological details of the sample (Figure 4, right panel).

To demonstrate the potential FDOCT for the imaging of the human retina *in vivo* as well as to visualize blood vascular structures at the human retina, we examined the left eye of one of authors (R.L. 31 years healthy eye). All measurements were performed with the aid of the differential FDOCT technique, therefore each optical A scan was reconstructed from two measured spectra.

Figure 5 presents *in vivo* retinal optical tomograms and sample A scans of the human eye. A central fragment of the healthy fovea is presented in panel a1. One of the A scans composing this tomogram is shown in panel a2. In Figure 5(b)

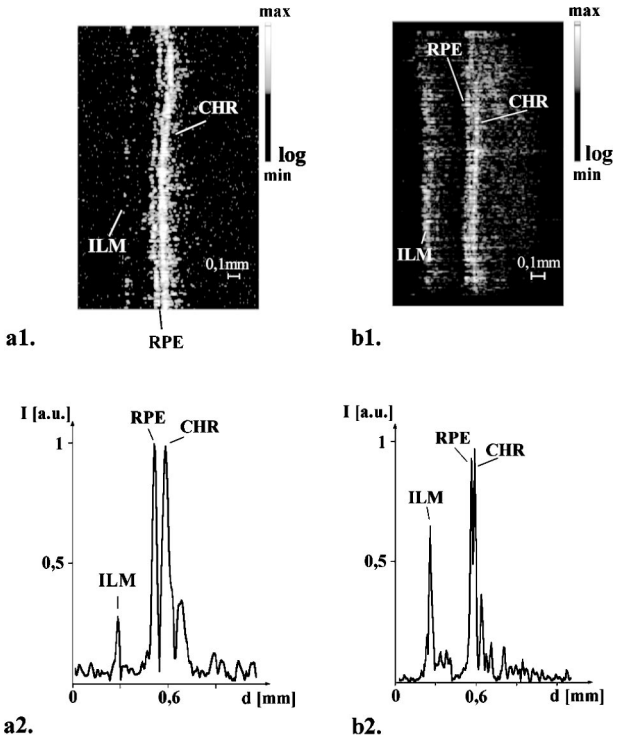

Fig. 5 Estimation of the retinal thickness. (a1) Tomogram of the human foveal pit *in vivo*, (b1) Tomogram of the human retina (detail of the central retina) *in vivo*, (a2), (b2) A scans extracted from the earlier tomograms as a function of the intensity of reflected light (arbitrary units) vs optical distance. ILM—inner limiting membrane, RPE—retinal pigment epithelium, CHR—choroid.

an example of the region of the central retina outside the macula lutea together with a representative A scan are shown. In accordance with other authors[29,30] we can identify the following retinal interfaces in the optical A scans: ILM—inner limiting membrane, RPE—retinal pigment epithelium, CHR—choroid.

The measured free space optical distance from the ILM to the retinal pigment epithelium RPE in the foveal pit is approximately 220 μm. Division of this optical thickness by the group refractive index of the retina (assumed value is 1.4) yields a geometrical thickness of approximately 160 μm. The average geometrical retinal thickness in the fovea taken from a textbook[31] is 130 μm. The free space optical thickness of the retina (ILM–RPE distance) including all seven layers outside the macula amounts to approximately 300 μm. The approximate geometrical thickness calculated with the earlier mentioned refractive index value is 215 μm. The average geometrical retinal thickness outside of fovea, as determined by other authors,[32] varies from 150 to 300 μm.

Examples of the human optic disk imaging *in vivo* are shown in Figure 6. There are three measurements of the same region with different transversal increment. The scanning was performed along the papillomacular axis. The exact position of the beam slightly changes from one measurement to another, however, anatomical details are recurrent. One can distinguish horizontal bands of relatively high (bright bands) and low reflectivity (dark band). It was already shown, by time domain techniques,[29] that higher reflectivity areas correspond

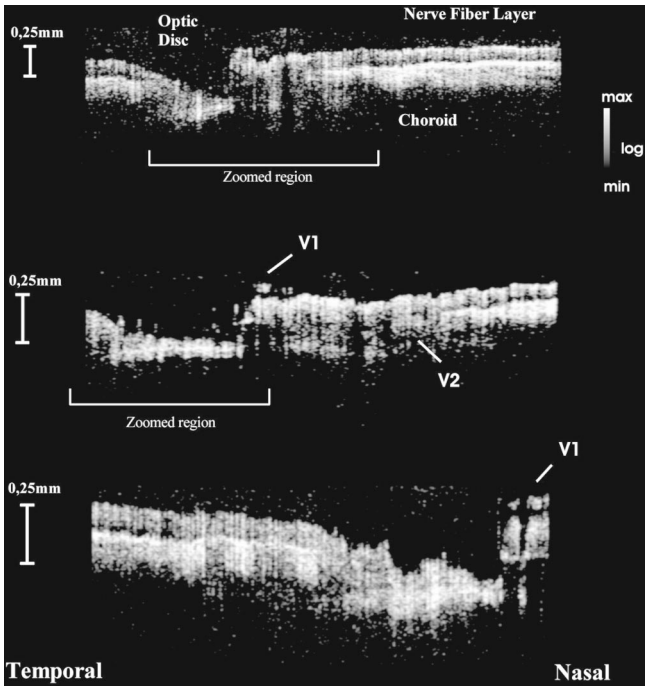

Fig. 6 Set of three optical tomograms of human retinal optic disk *in vivo*. Each tomogram was measured independently with the variable transversal scan increment. The zoomed region bar depicts coarse scanning range expanded for each next tomogram. V1 and V2 show structures, which resemble blood vessels.

to the nerve fiber layer RNFL and choroid CHR together with the retinal pigment epithelium RPE, while the nuclear layers and the inner and outer segments of photoreceptor demonstrate low reflectivity. The characteristic convergence of the relative high reflectivity layers at the left edge of the optic disk indicates that the bright areas mainly correlate to the nerve fibers, which shall be dominating in this region. The optic disk is the point where all nerves and veins leave the eyeball. Hence, the probability of vein imaging in this region is high. The oval structures V1 (ϕ approximately $=150\ \mu$m) and V2 (ϕ approximately$=400\ \mu$m) are probably sections of blood vessels.

The dFDOCT tomogram of the macular region is shown in the Figure 7. Again the transversal scanning was done along the papillomacular axis. The inner bright band almost disappears in the foveal pit. Therefore, one can assume that this band corresponds to the fiber nerve layer. Directly below the foveal pit a single bright strip is distinguishable. Hypothetically we can link this structure to the retinal pigment epithelium layer.

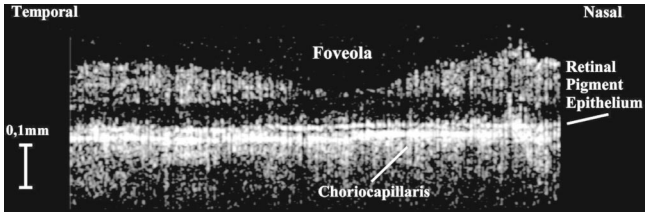

Fig. 7 Tomogram of cross-section of the human retinal macula *in vivo* obtained by differential FDOCT.

Unavoidable eye movements caused that the adjacent A scans might be misaligned with respect to each other. In case of macular imaging due to pronounced reflex of the pigment epithelium it is possible to apply a cross-correlation technique[7] in order to realign the consecutive optical A scans.

6 Discussion

We demonstrated the possibility of morphological ophthalmologic imaging with the aid of a modified FDOCT technique. It was shown that differential FDOCT produces images which are free of parasitic autocorrelation terms, with the drawback of effectively doubling the acquisition time. For the 16 bit CCD system in use the data transfer of 1024 spectral points to the personal computer needed 19 ms. Hence, with dFDOCT we need approximately 40 ms for one optical A scan. The total 500×500 tomographic image takes about 20 s. Faster CCD systems on the market allow for a 1 MHz/pixel transfer rate. This reduces the acquisition time for one 500×500 pixel tomogram to 1 s, which is sufficient for clinical applications.

In both FDOCT and time domain OCT the resolution of the system depends on the same factors. In our system the transversal resolution can be improved by increasing the aperture of the incident beam. This is achieved by reducing the focal length of the object lens. The longitudinal resolution can be easily improved by using light sources with broader spectral bandwidths.

The shot noise level is achieved by introduction a reference signal of sufficient intensity but within a saturation limit. The saturation level of CCD detector is many orders of magnitude lower than for photodiodes. Still, the shot noise level in our system is easily reached[33] due to the inherently low dark and read noise figures of CCDs. This fact can be also demonstrated experimentally by switching off the camera cooling system—the increase of thermal noise does not deteriorate the FDOCT image quality. In our system we experimentally determined the dynamic range to be 71 dB, whereas for temporal systems calculated value above 100 dB were reported.[28,34] Despite this considerable difference the quality of the presented retinal tomograms obtained by FDOCT are not much worse than the best time domain OCT retinal images.[35] This apparent contradiction may be explained by the following observation: The dynamic range that is necessary to distinguish between retinal layers essential for ophthalmologic diagnosis (retinal nerve fiber layer, photoreceptor layer and pigment epithelium layer)[8] is approximately equal to 40 dB, which lies well within the dynamic range of our FDOCT system.

7 Summary

In conclusion, we have demonstrated the first *in vivo* tomograms of the human retina obtained by Fourier domain optical coherence tomography. We were able to visualize details of the macula and optic disk *in vivo*. A quantitative estimation of the thickness of different retinal layers was presented. The results appear competitive to the retinal tomograms obtained by conventional OCT instruments, that are based on a time-domain measurement setup.

Acknowledgments

The authors thank J. Anuszkiewicz, J. Kowalski, H. Schiller, and J. Wojtylewski from the mechanical workshop of NCU Physics Institute for their professional support. This research was supported by the Grant No. UMK 502-F and an exchange program financed by the Oesterreichische Akademische Austauschdienst (OEAD) together with the Polish State Committee for Scientific Research (Grant No. 10/2001).

References

1. R. H. Webb, ''Scanning laser ophthalmoscope,'' in *Noninvasive Diagnostic Techniques in Ophthalmology*, B. R. Masters, ed., pp. 438–450, Springer, New York (1990).
2. K. Emi, Y. Kobayashi, S. Chujo, C. Fujioka, and M. Yokoyama, ''The biometry of each thickness of the human retina, choroid and sclera by using ultrasound and Fourier analysis at the foveola,'' *Nippon Ganka Gakki Zasshi* **87**, 74–79 (1983).
3. A. F. Fercher, K. Mengedoht, and W. Werner, ''Eye length measurement by interferometry with partially coherent light,'' *Opt. Lett.* **13**, 186–189 (1988).
4. A. Roorda and D. R. Williams, ''New directions in imaging the retina,'' *Opt. Photonics News* **8**, 23–29 (1997).
5. D. Huang, E. A. Swanson, C. P. Lin, J. S. Schuman, W. G. Stinson, W. Chang, M. R. Hee, T. Flotte, K. Gregory, C. A. Puliafito and J. G. Fujimoto, ''Optical Coherence Tomography,'' *Science* **254**, 1178–1181 (1991).
6. A. F. Fercher, C. K. Hitzenberger, W. Drexler, G. Kamp, and H. Sattmann, ''*In vivo* optical coherence tomography,'' *Am. J. Ophthalmol.* **116**, 113–114 (1993).
7. E. A. Swanson, J. A. Izatt, M. R. Hee, D. Huang, C. P. Lin, J. S. Schuman, C. A. Puliafito, and J. G. Fujimoto, ''*In vivo* retinal imaging by optical coherence tomography,'' *Opt. Lett.* **18**(21), 1864–1866 (1993).
8. C. A. Puliafito, M. R. Hee, C. P. Lin, E. Reichel, J. S. Schuman, J. S. Duker, J. A. Izatt, E. A. Swanson, and J. G. Fujimoto, ''Imaging of macular diseases by optical coherence tomography,'' *Ophthalmology (Philadelphia)* **102**(2), 217–229 (1995).
9. M. R. Hee, C. A. Puliafito, J. S. Duker, E. Reichel, J. G. Coker, J. R. Wilkins, J. S. Schuman, E. A. Swanson, and J. G. Fujimoto, ''Topography of diabetic macular edema with optical coherence tomography,'' *Ophthalmology (Philadelphia)* **105**(2), 360–370 (1998).
10. M. R. Hee, C. A. Puliafito, C. Wong, J. S. Duker, E. Reichel, J. S. Schuman, E. A. Swanson, and J. G. Fujimoto, ''Optical coherence tomography of macular holes,'' *Ophthalmology (Philadelphia)* **102**(5), 748–756 (1995).
11. M. R. Hee, C. A. Puliafito, C. Wong, E. Reichel, J. S. Duker, J. S. Schuman, E. A. Swanson, and J. G. Fujimoto, ''Optical coherence tomography of central serious chorioretinopathy,'' *Am. J. Ophthalmol.* **120**(1), 65–74 (1995).
12. J. S. Schuman, M. R. Hee, C. A. Puliafito, C. Wong, T. Pedut-Kloitzman, C. P. Lin, E. Hertzmark, J. A. Izatt, A. Swanson, and J. G. Fujimoto, ''Quantification of nerve fiber layer thickness in normal and glaucomatous eyes using optical coherence tomography,'' *Arch. Ophthalmol. (Chicago)* **113**, 586–596 (1995).
13. U. Morgner, W. Drexler, F. X. Kärtner, X. D. Li, C. Pitris, E. P. Ippen, and J. G. Fujimoto, ''Spectroscopic optical coherence tomography,'' *Opt. Lett.* **25**(2), 111–113 (2000).
14. R. Leitgeb, M. Wojtkowski, C. K. Hitzenberger, M. Sticker, A. Kowalczyk, and A. F. Fercher, ''Spectral Measurement of Absorption by Spectroscopic Frequency-Domain OCT,'' *Opt. Lett.* **25**(11), 820–822 (2000).
15. A. F. Fercher, C. K. Hitzenberger, G. Kamp, and S. Y. El-Zaiat, ''Measurements of intraocular distances by backscattering spectral interferometry,'' *Opt. Commun.* **117**, 43–48 (1995).
16. A. F. Zuluaga and R. Richards-Kortum, ''Spatially resolved spectral interferometry for determination of subsurface structure,'' *Opt. Lett.* **24**, 519–521 (1999).
17. Th. Dresel, G. Hausler, and H. Venzke, ''Three-dimensional sensing of rough surfaces by coherence radar,'' *Appl. Opt.* **31**, 919–925 (1992).
18. A. Eigensee, G. Hausler, J. M. Hermann, and M. W. Lindner, ''A new method of short coherence interferometry in human skin (*in vivo*) and in solid volume scatterers,'' *Proc. SPIE* **2925**, 169–178 (1996).
19. F. Lexer, C. K. Hitzenberger, A. F. Fercher, and M. Kulhavy, ''Wavelength tuning interferometry of intraocular distances,'' *Appl. Opt.* **36**(25), 6548–6553 (1997).
20. U. H. P. Haberland, V Blazek, and H. J. Schmitt, ''Chirp Optical Coherence Tomography of layered scattering media,'' *J. Biomed. Opt.* **3**(3), 259–265 (1998).
21. I. Zeylikowich, A. Gilerson, and R. R. Alfano, ''Nonmechanical grating-generated scanning coherence microscopy,'' *Opt. Lett.* **23**(23), 1797–1799 (1998).
22. ''American national standard for safe use of lasers,'' ANSI Z 136.1, American National Standard Institute, New York (1993).
23. M. Born and E. Wolf, *Principles of Optics*, 7th ed., Cambridge University Press, Cambridge (1999).
24. J. W. Goodman, *Statistical Optics*, Wiley, New York (1985).
25. G. Hausler and M. W. Lindner, ''Coherence radar and spectral radar—New tools for dermatological diagnosis,'' *J. Biomed. Opt.* **3**(1), 21–31 (1998).
26. A. F. Fercher, ''Optical coherence tomography,'' *J. Biomed. Opt.* **1**(2), 157–173 (1996).
27. P. Andretzky, M. W. Lindner, J. M Hermann, A. Schultz, M. Konzog, F. Kiesewetter, and G. Hausler, ''Optical coherence tomography by *spectral radar*: dynamic range estimation and in vivo measurements of skin,'' *Proc. SPIE* **3567**, 78–87 (1998).
28. E. A. Swanson, J. A. Izatt, D. Huang, M. R. Hee, J. G. Fujimoto, C. P. Lin, and C. A. Puliafito, ''High-speed optical coherence domain reflectometry,'' *Opt. Lett.* **17**(2), 151–153 (1992).
29. C. A. Toth, D. G. Narayan, S. A. Boppart, M. R. Hee, J. G. Fujimoto, R. Birngruber, C. P. Cain, C. D. DiCarlo, and W. P. Roach, ''A comparision of retinal morphology viewed by optical coherence tomography and light microscopy,'' *Arch. Ophthalmol. (Chicago)* **115**(11), 1425–1428 (1997).
30. A. Baumgartner, C. K. Hitzenberger, H. Satmann, W. Drexler, and A. F. Fercher, ''Signal and resolution enhancements in dual beam optical coherence tomography of the human eye,'' *J. Biomed. Opt.* **3**(1), 45–54 (1998).
31. H. Hogan, J. A. Alvarado, and J. E. Weddell, *Histology of Human Eye. An Atlas and Textbook*, WB Saunders, Philadelphia (1971).
32. W. Drexler, C. K. Hitzenberger, H. Satmann, and A. F. Fercher, ''Measurement of the thickness of fundus layers by partial coherence tomography,'' *Opt. Eng.* **34**(3), 701–710 (1995).
33. Catalogue Oriel Instruments, ''New multichannel detection systems,'' pp. 2–5 (1998).
34. X. J. Wang, T. E. Millner, and J. S. Nelson, ''Characterization of fluid flow velocity by optical Doppler tomography,'' *Opt. Lett.* **20**, 1337–1339 (1995).
35. W. Drexler, R. K. Ghanta, J. S. Schuman, T. Ko, U. Morgner, F. X. Kartner, and J. G. Fujimoto, ''*In vivo* optical biopsy of the human retina using optical coherence tomography,'' *Proc. SPIE* **4251**, 183–187 (2001).